X-723-74-243
PREPRINT

NASA TM X- 70753

VARIABLE CO_2 LASER ATTENUATOR

BERNARD J. KLEIN
JOHN J. DEGNAN
HAROLD E. WALKER
THOMAS ZAGWODZKI

AUGUST 1974

GSFC — GODDARD SPACE FLIGHT CENTER —
GREENBELT, MARYLAND

X-723-74-243

VARIABLE CO_2 LASER ATTENUATOR

Bernard J. Klein
John J. Degnan
Harold E. Walker
Thomas Zagwodzki

August 1974

GODDARD SPACE FLIGHT CENTER
Greenbelt, Maryland

VARIABLE CO_2 LASER ATTENUATOR

ABSTRACT

An infrared wavelength variable attenuator based on contra-rotating germanium wedges is examined theoretically. The device redirects the paths of internal reflections associated with an optical flat to avoid closely spaced parallel beams at the output. Complementary wedges separated by an air gap compose an "optical flat" which, when combined with a masking arrangement, restricts unwanted reflections. A model of the device has been built and experimentally evaluated. The results compare favorably with the dynamic range of attenuation of 2 to 50 dB from theoretical calculations, and show a substantial reduction in the etalon effect associated with pairs of optical flats.

CONTENTS

LIST OF ILLUSTRATIONS

VARIABLE CO_2 LASER ATTENUATOR

I. INTRODUCTION

Communications, tracking, and radiometer systems are under development which exploit the infrared portions of the electromagnetic spectrum. Whenever a new portion of the spectrum is opened for such applications, the development of experimental and operational systems must be supported by the development of auxiliary instrumentation which aids in systems research and test. A common requirement in any such system research and development is a calibrated means of adjusting the signal or local oscillator power levels. This report describes a variable attenuator for the infrared wavelengths - particularly the 10.6-μm wavelength of the CO_2 laser.

Some possible techniques for the attenuation of 10.6 μm have been presented by a number of authors. A double prism arrangement was suggested by Leeb[1]. The device appears useful for any polarization of the beam and has a large range of attenuation. although, for the lower ranges, maintaining the parallel alignment of the prisms can be difficult. Abrams and Gandrud[2] proposed a system using a $\lambda/4$ plate and Brewster window. Although, this system works well for linearly polarized beams, it substantially redirects the beam. Thus, it cannot be simply inserted into the beam path of an existing system without the use of additional mirrors. GTE Sylvania has a commercially available CO_2 laser attenuator, but this device changes the polarization of the beam; an undesirable characteristic for use with heterodyne detection. In 1969, McElroy, et al., described[3] a 10.6-μm variable attenuator for linearly polarized light based on contra-rotating optical flats. This idea was proposed by Sporton[4] to keep the incident beams from suffering a lateral displacement. McElroy proposed the use of four optical flats to extend the range of attenuation. An inherent problem with this system is that multiple internal reflections become significant at angles of incidence far from the Brewster's angle, and cause interference effects to take place within the primary output beam. This interference is commonly known as the etalon effect. Sporton used antireflection coatings to suppress the etalon effect within the optical flats, but he tabulated his results for approximately two degree increments in the angle of incidence. The use of 0.5 degree or smaller increments would have shown that the amplitude transmission coefficient is not strictly monotonic as implied by his results.

II. OPTICAL ATTENUATOR DESIGN

Consider a beam of linearly polarized light to be incident upon an optical flat of refractive index n_1, at an angle of incidence α. The beam is refracted within the flat at an angle β and suffers multiple reflections. The extraneous beams resulting from the reflections exit the flat parallel to the primary output beam (first beam). (See Fig. 1). When α is far from the Brewster's angle of the optical material, the multiple reflections become significant and begin to interfere with the main output beam. The overlap of these closely spaced parallel beams produces an etalon effect.

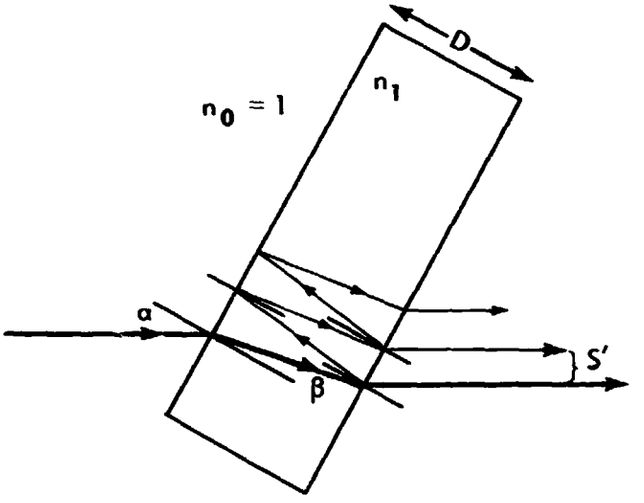

Figure 1. Reflections within an optical flat of width D and index of refraction n_1.

To eliminate the closely spaced parallel beams, an optical wedge was used instead of a flat. Internal reflections will not exit the wedge parallel to the main beam, but at different angles. In fact, as the angle α is increased, the higher order reflections very quickly begin to exit at much greater angles. If the wedge is combined with its complement, and separated by an air gap of width d as in Fig. 2, the primary beam will exit along a path parallel to the incident beam. If two parallel optical flats instead of two wedges were used, the number of extraneous parallel beams would be increased. The double wedge approach has nearly the same range of attenuation, but the influence of the etalon effect is reduced due to the change in the paths of the internally reflected beams. Reflections within the air gap do result in extraneous beams whose paths outside the composite flat are parallel to the main beam. However, as will be shown

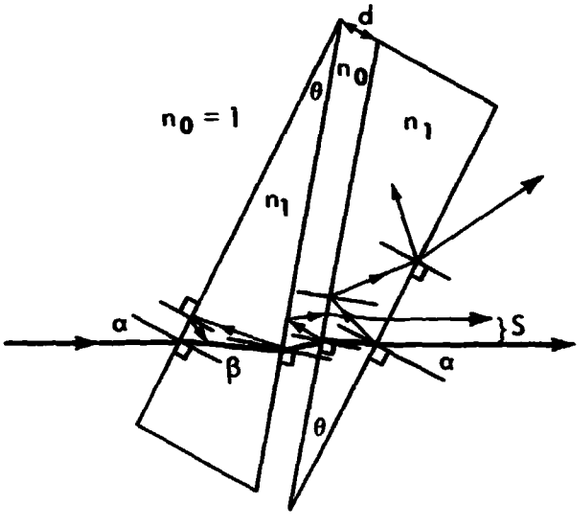

Figure 2. A pair of complementary wedges of index of refraction n_1, separated by an air gap of width d.

However, as will be shown later, the distance between the primary beam and the nearest extraneous parallel beam is sufficiently large so that a mask may be used to eliminate the unwanted beam.

The width D of the flat in Fig. 1 and the size of the wedge angle α in Fig. 2 are greatly exaggerated to clarify the effects of the designs. To make the distance S' between the primary and "secondary" beams in Fig. 1 as large as possible, one might increase the thickness of the flat, but it would be costly to obtain a homogeneous material of sufficient thickness.

Germanium was chosen to be the attenuating material because it gives the widest range of attenuation and truly homogeneous optical flats of reasonable size are available. Germanium's high refractive index ($n_1 = 4.0$) results in a Brewster angle ($\alpha_B = \mathrm{Tan}^{-1} n_1$) of approximately 76° and dictates a large useful range of incidence angles from 0° to 76°.

The design of the double wedge system was made under certain physical restrictions, since a redesign of an existing device shown in Fig. 3 was involved. First, the aperture mounts had to be made thinner to accomodate an angle of tilt of 76 degrees. This change further limited the width of the air gap, d, which is the main parameter in separating the parallel beams. It will be shown later that enlarging d increases the distance S, in Fig. 2, proportionally. However, a very

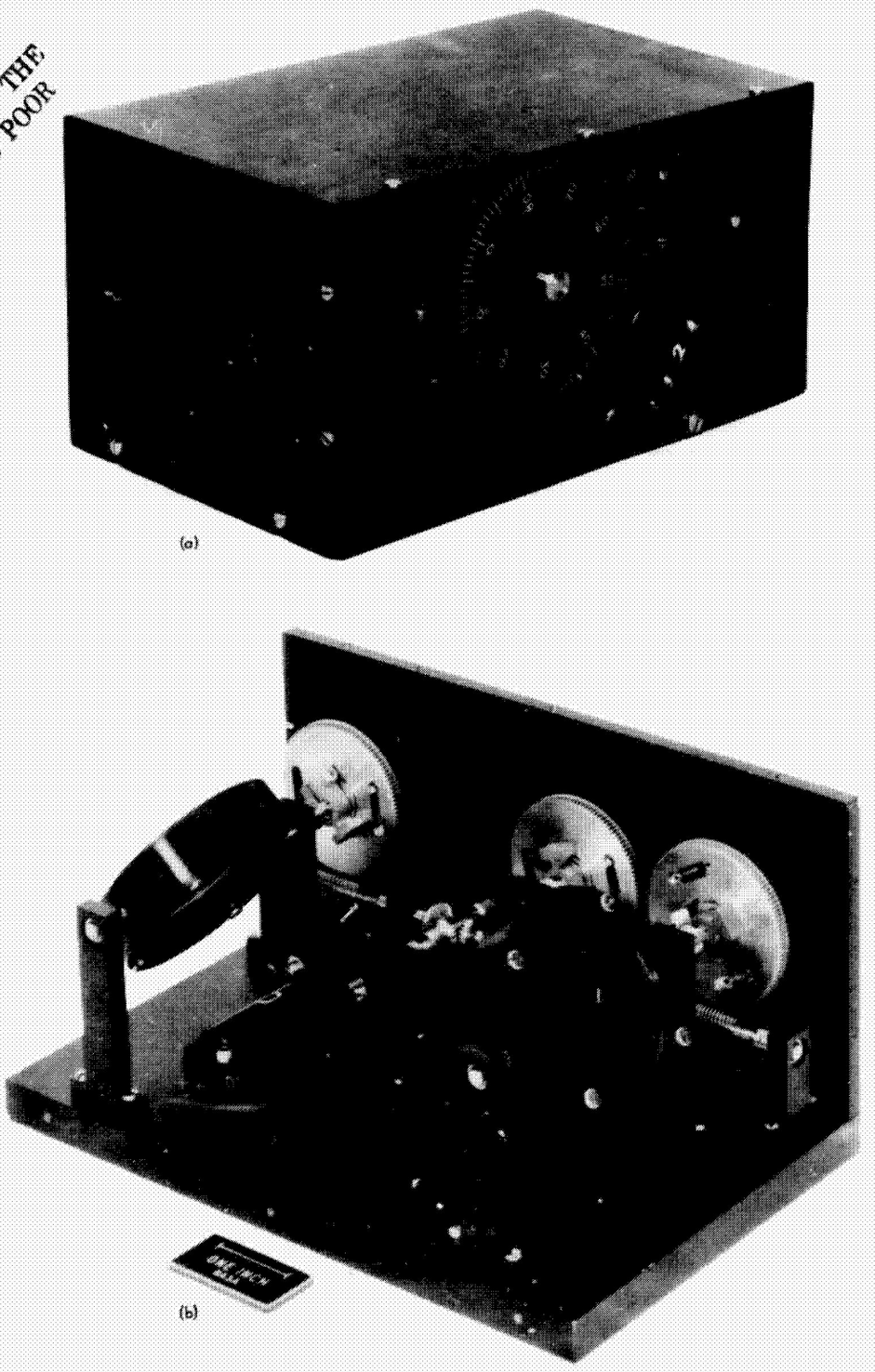

Figure 3. Precision variable attenuator (a) View with the cover on showing the dial and vernier scale which records the angle of tilt. (b) View with the cover off.

large air gap may require the aperture of the wedges to be increased for the system to contain the beam. The wedge angle θ was chosen sufficiently large to efficiently eliminate the internally reflected beams and yet small enough to avoid excessively limiting the air gap width. An angle of 1° was felt to be a good compromise. With this choice of angle the air gap width was restricted to a maximum size of .55 cm by the physical dimensions of the mounts.

The distances S' and S can be calculated in terms of variable parameters. From Fig. 1, S' is given by

$$S' = \frac{2 \cdot D \cdot \mathrm{Sin}\,\alpha\,\mathrm{Cos}\,\alpha}{(n_1^2 - \mathrm{Sin}^2\,\alpha)^{1/2}} \tag{1}$$

From Fig. 2, an equation for S can be derived (Appendix A), i.e.,

$$S = 2d\,\mathrm{Cos}\,\theta\,\mathrm{Tan}\,\gamma\,\mathrm{Cos}(\beta - \theta)\frac{\mathrm{Cos}\,\alpha}{\mathrm{Cos}\,\beta} \tag{2}$$

where

$$\beta = \mathrm{Sin}^{-1}\left(\frac{\mathrm{Sin}\,\alpha}{n_1}\right)$$

$$\gamma = \mathrm{Sin}^{-1}\left[n_1\,\mathrm{Sin}(\beta - \theta)\right]$$

Using Eqs. (1) and (2), the improvement on the distance S' that is obtained by going to the wedge structure can be clearly shown. For purposes of comparison, consider the widths D and d in Figures 1 and 2 respectively to be the same, i.e. D = d. Letting d be the particular value of 0.55 cm, $\theta = 1^{\circ}$, and $n_1 = 4.0$ Eqs. (1) and (2) were plotted in Fig. 4 to show that there is a substantial increase in the distance between the primary output beam and its closest extraneous parallel beam. From Fig. 4, one can observe that for the complementary wedges the "secondary" is below the main beam and passes through the primary beam at approximately an angle of tilt of four degrees. For a particular range of α it is possible to physically block the "secondary" beam by using a masking arrangement. This assumes, of course, that the beam diameters are small.

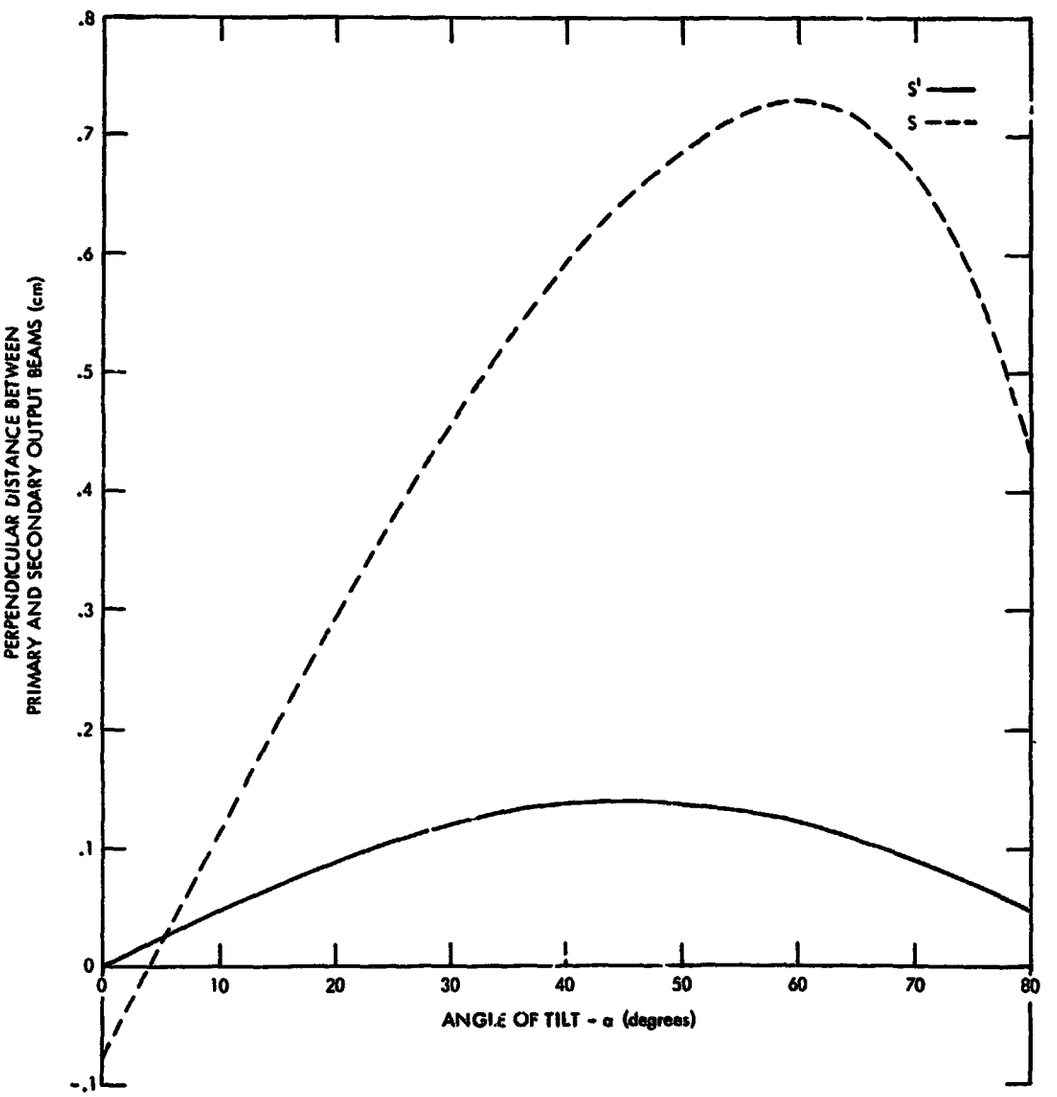

Figure 4. Relative distance, S' and S, between the primary and first internally reflected parallel output beams for the optical flat and the composite flat respectively.

It is obvious from Fig. 2, that the output beam suffers a variable displacement from its original direction along the optical axis, which is defined by the laser beam through the centers of the composite flats. However, two sets of wedges, placed as in Fig. 5, and moving in contra-rotation, allows no net displacement of the beam.

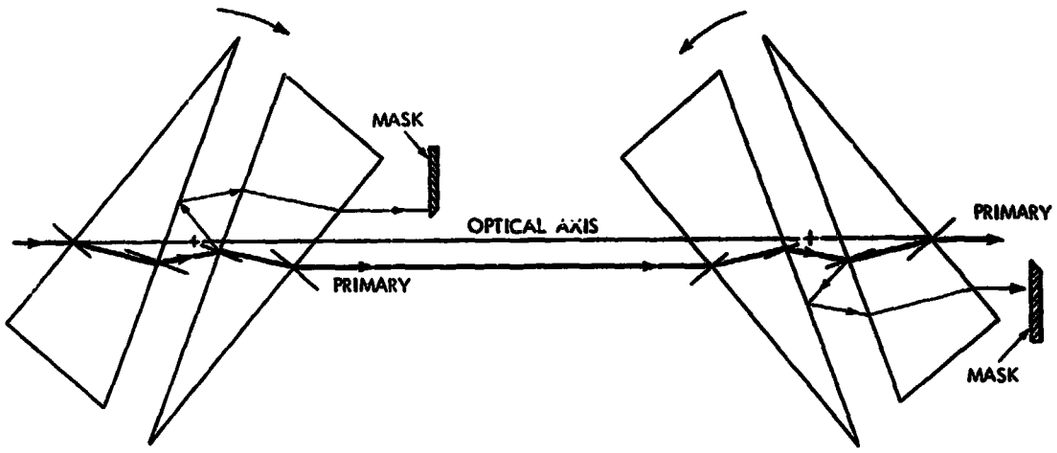

Figure 5. A pair of composite flats arranged to move in contra-rotation to keep the primary beam from suffering a lateral displacement. Also shown are the positions for stationary masks used to block extraneous reflected beams.

Fig. 5 also suggests the location for a pair of masks to block the "secondary" beams. The masking material can be any rigid material which will absorb the radiation, e.g., anodized aluminum or black plastic, both of which should be given flat finishes. As mentioned above, the primary output beam of the first composite flat in Fig. 5 is displaced from the optical axis. A calculation of this variable distance (Appendix B) shows that the beam moves downward monotonically from the axis as the angle of tilt increases. Remembering that the beam is not infinitely thin as depicted in the figures, stationary masks can be placed close to the optical axis, allowing for the radius of the main beam to avoid clipping of its energy. If a mask does not block the "secondary" beams from the first pair of wedges they would enter the second composite flat and exit the attenuator collinear with the main beam.

Ideally, the first mask would be allowed to change its position, moving downward at the same increments as the primary beam. This would aid in blocking the secondary, which begins to move in the opposite direction. In its stationary position, the secondary does not rise high enough until $\alpha \approx 20°$ for the mask to become effective.

A drawing of the entire opto-mechanical system without the masks is shown in Fig. 6. The composite flats move in contra-rotation by means of a crank connected to a differential driving mechanism and a limit stop assembly. The differential, spur and worm gears are all antibacklash gears which help to insure an accurate angle of tilt and repeatability. The angle of incidence of the composite flat is read from a dial which operates through a gear ratio arrangement. The dial with a 0.1 degree vernier is shown in Fig. 3a. The angle of incidence was estimated to be resettable within 0.1 degree.

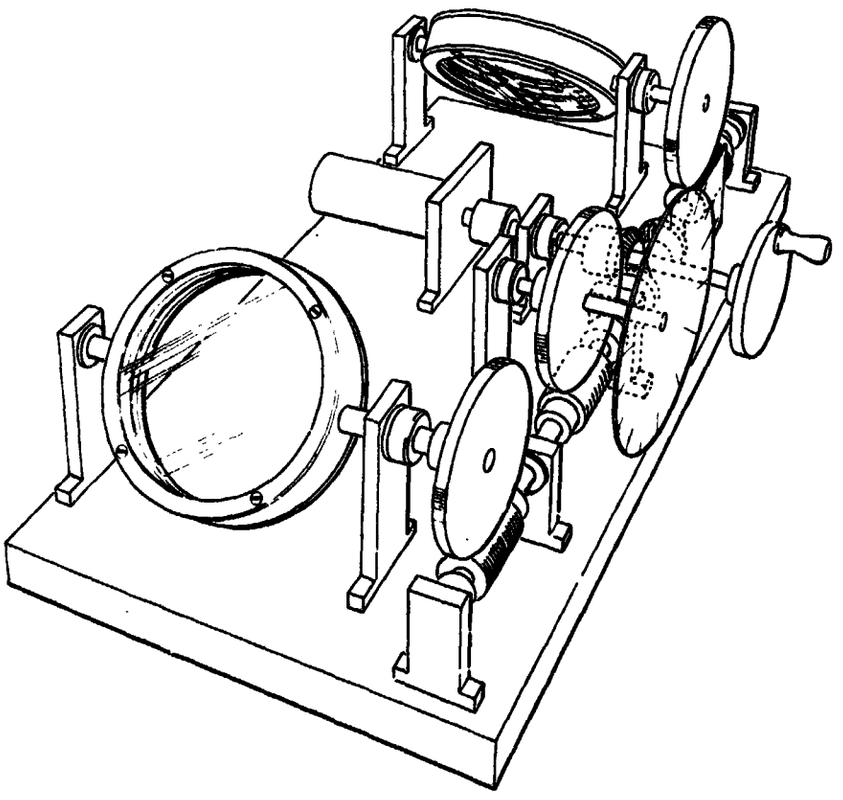

Figure 6. Drawing of variable CO_2 laser attenuator without the cover and masks.

III. TRANSMISSION THROUGH THE COMPOSITE FLAT

The power transmitted in the main beam through one composite flat can be shown to be[5]

$$T_n = \left[\frac{4n_1 \operatorname{Cos} \alpha \operatorname{Cos} \beta}{(n_1 \cos \beta + \operatorname{Cos} \alpha)^2} \quad \frac{4n_1 \operatorname{Cos} \tau \operatorname{Cos} \gamma}{(n_1 \operatorname{Cos} \tau + \operatorname{Cos} \gamma)^2} \right]^2$$

and

$$T_p = \left[\frac{4n_1 \operatorname{Cos} \alpha \operatorname{Cos} \beta}{(n_1 \operatorname{Cos} \alpha + \operatorname{Cos} \beta)^2} \cdot \frac{4n_1 \operatorname{Cos} \tau \operatorname{Cos} \gamma}{(n_1 \operatorname{Cos} \tau + \operatorname{Cos} \gamma)^2} \right]^2$$

where T_n and T_p refer to the cases in which the incident beam's plane of polarization is normal and parallel to, respectively, the plane of incidence. The angles α and γ are the angles of incidence and refraction respectively, and $\tau = \beta - \theta$.

Power losses due to absorption within the material are given by a factor

$$e^{-\xi \ell}$$

where ξ is the absorption coefficient of the material and ℓ is the optical path length through the material. For the polycrystalline germanium, the absorption coefficient is 0.055 (Ref. 6).

The transmission through both composite flats for the two cases is

$$\mathfrak{I}_n = (T_n e^{-\xi \ell_1} \cdot e^{-\xi \ell_2})^2 \tag{3}$$

and

$$\mathfrak{I}_p = (T_p e^{-\xi \ell_1} \cdot e^{-\xi \ell_2})^2 \tag{4}$$

with ℓ_1 and ℓ_2 being the path lengths of the light in each wedge (see Appendix C for the mathematical representation of these variables). $\mathfrak{I}_p$ has been plotted, on a linear scale in Fig. 7 and in dB in Fig. 8, as the theoretical performance curves of the attenuator. $\mathfrak{I}_n$ has been plotted in Figs. 9 and 10 for the normally polarized case.

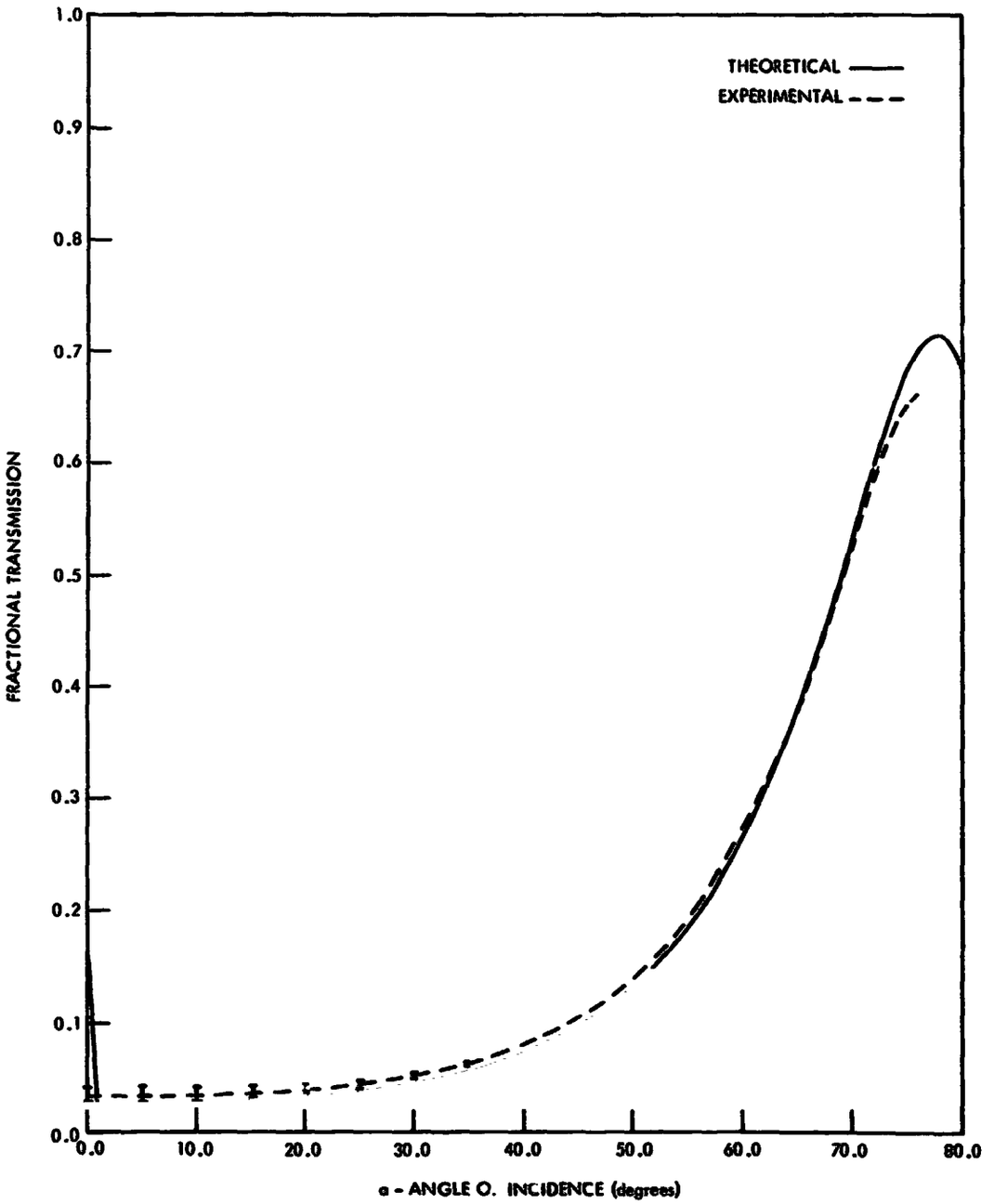

Figure 7. Theoretical ($\mathfrak{I}_p$) and experimental linear transmission curves relating the performance of the composite flat attenuator, with the masking arrangement shown in Fig. 4, for the E-field parallel to the plane of incidence.

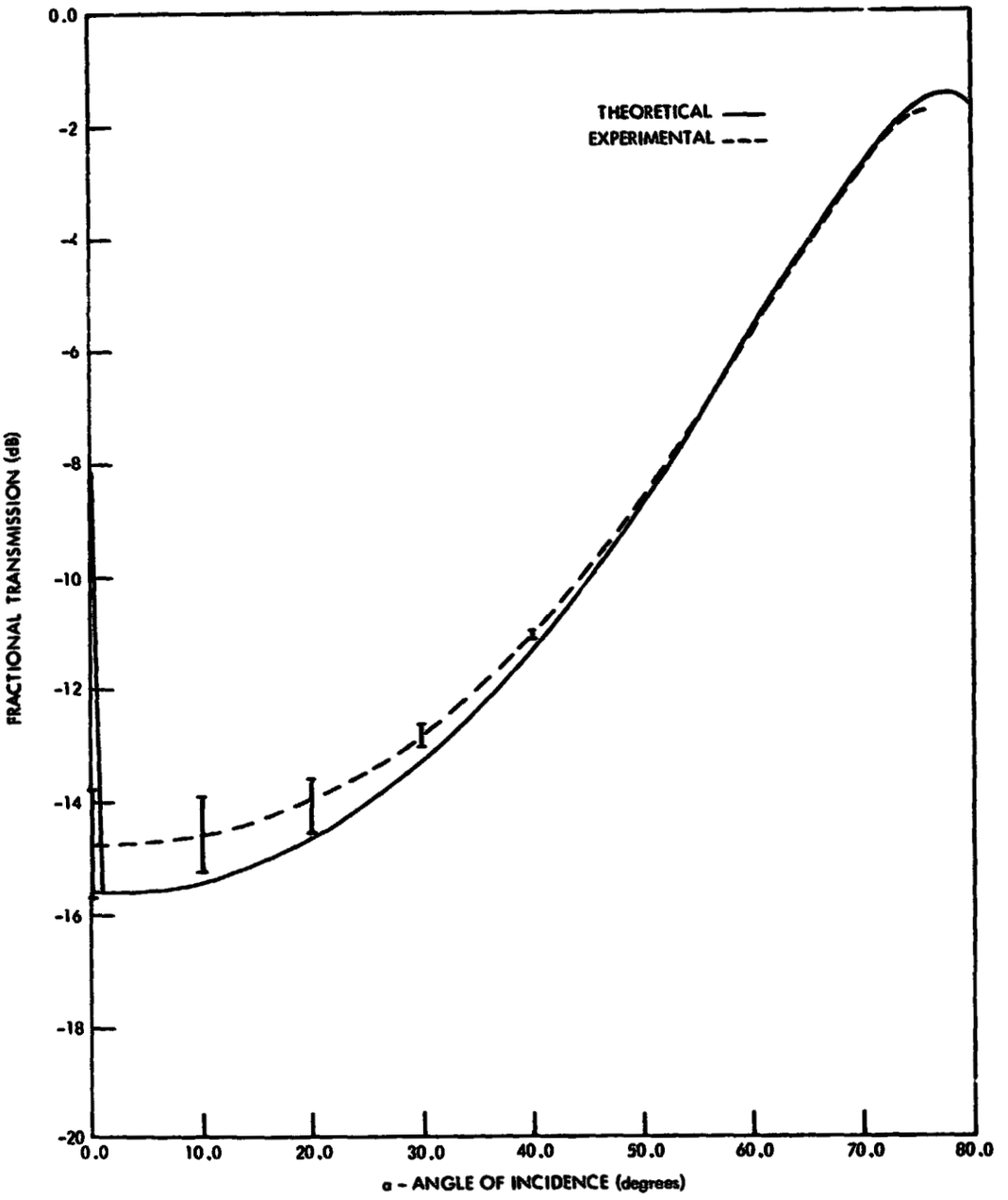

Figure 8. Theoretical and experimental transmission curves in dB for the E-field parallel to the plane of incidence.

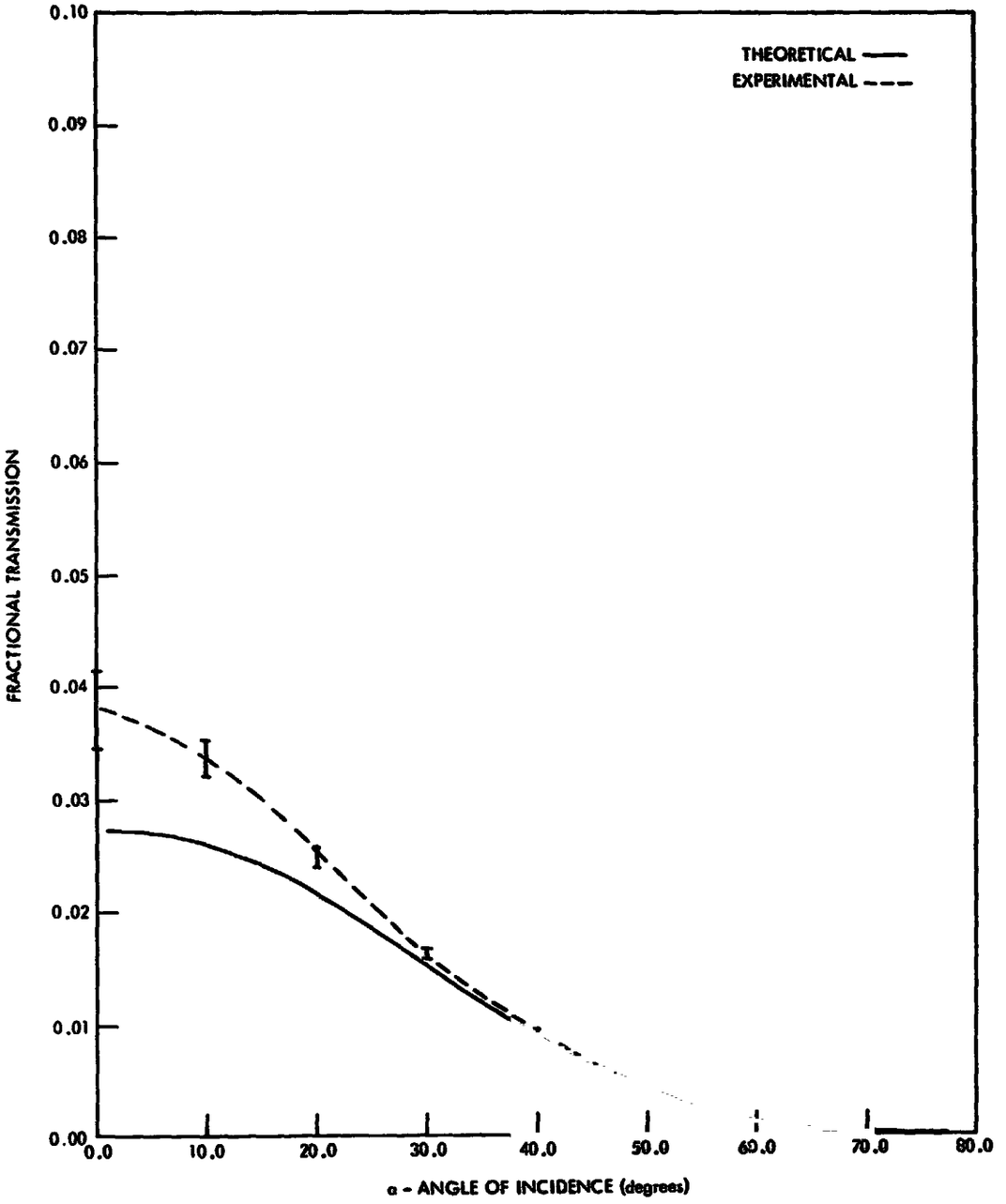

Figure 9. Theoretical (τ_n) and experimental linear transmission curves relating the performance of the composite flat attenuator, with the masking arrangement shown in Fig. 4, for the E-field normal to the plane of incidence.

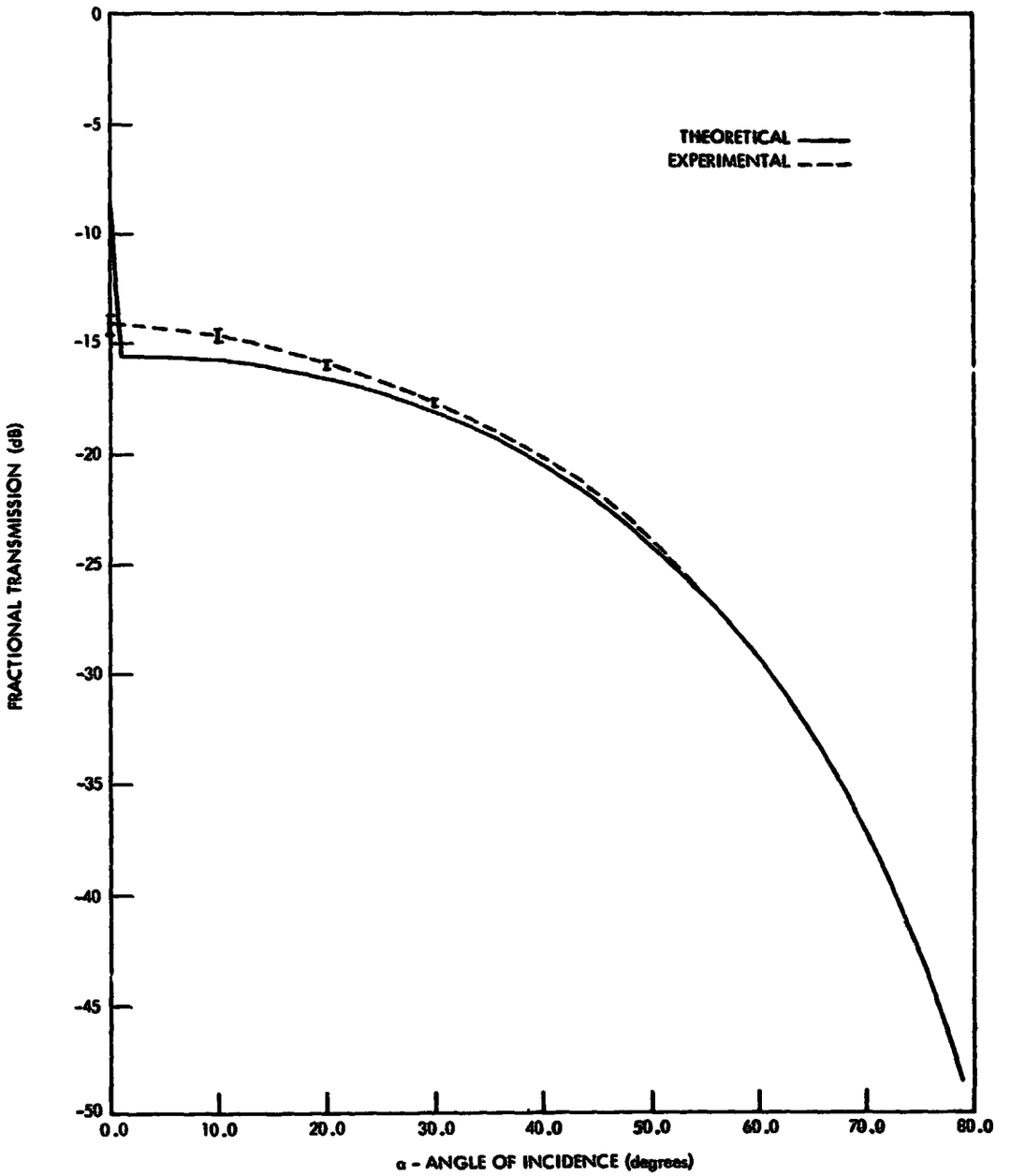

Figure 10. Theoretical and experimental transmission curves in dB for the E-field normal to the plane of incidence.

IV. EXPERIMENTAL RESULTS

Measurements were made using a CO_2 laser. The angle of incidence was incremented by 0.25 degree steps from 0 to 76 degrees. Figures 7 and 8 are linear and dB plots, respectively, which show the theoretical predictions and experimental results for parallel polarized light. Figures 9 and 10 give results for normally polarized light.

All of the experimental data in Figs. 7 thru 10 for the wedge system attenuator was taken with the stationary masks in place and the curves represent an average of that data. The plots display the variation in attenuation by "error" bars. This variation is due to the etalon effect, and, as shown later, there is a marked decrease in this interference when compared to the attenuator composed of optical flats.

Figures 7 thru 10 show the range from $\alpha = 0$ to $\alpha = 25$ degrees, in which the etalon effect is prominent, to be a useless region for clean monotonic attenuation. However, it can be seen from the figures that the combined regions for both polarizations lost to useful attenuation comprise an area only 5 dB in width. For $\alpha > 74°$ the window mounts of the device began to obscure the beam, but this region accounts for only a small fraction of the attenuation range.

To show the reduction in the etalon effect we replaced the wedges of Fig. 5 with four germanium optical flats and plotted experimental data for the case of parallel polarized light. Both of the devices, composed of either the wedges or the flats, have approximately the same range of attenuation. Figure 11 is a plot of the performance of an attenuator composed of two pairs of optical flats. The thickness of each flat was 0.50 cm.

Clearly, from the figure, the etalon effect is present throughout a range of α from 0 to 65 degrees. The mounts holding the flats obscured the beam at higher values of α, but we would expect the amplitude of the interference to become much less as α approaches 76°. Figure 12 depicts the experimental performance for the attenuator using the wedge system and the stationary masks; and it shows a substantial reduction in the interference throughout the range of α when compared to the attenuator utilizing four flats.

The extraneous beam which accounts for most of the interference at the output of the attenuator is attributed to the reflection in the air gap between the second pair of wedges. This secondary beam was incorporated into the calculation of $\mathfrak{I}_p$ of Eq. (4). A diameter of 0.6 cm was assumed for the beam, and its effect is shown in Fig. 13. The experimental result of Fig. 12 coincides extremely well with the prediction of Fig. 13, although in the lower range of α better agreement may have been attained if more extraneous parallel beams were considered in the analysis.

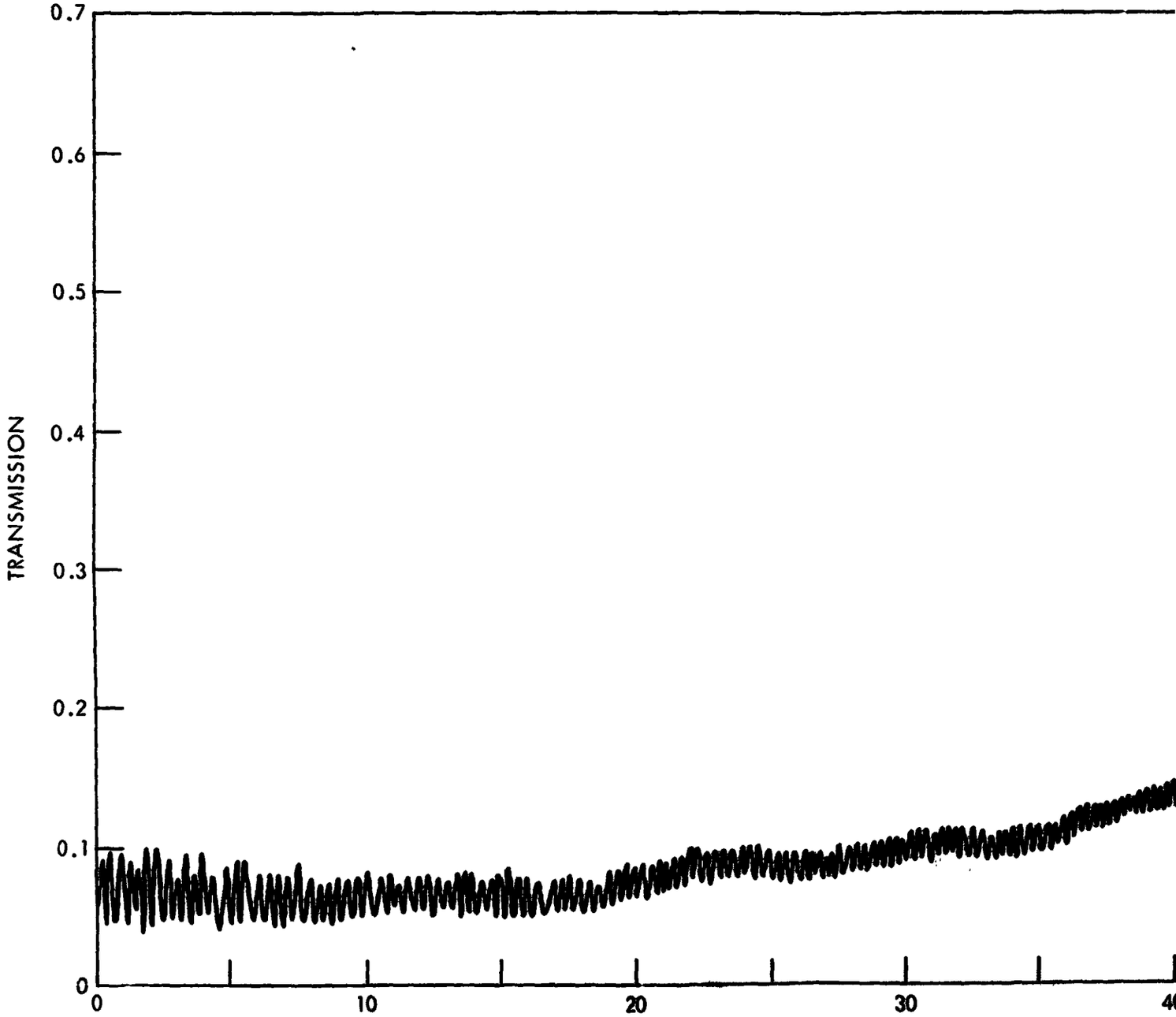

Figure 11. Experiment

FOLDOUT FRAME /

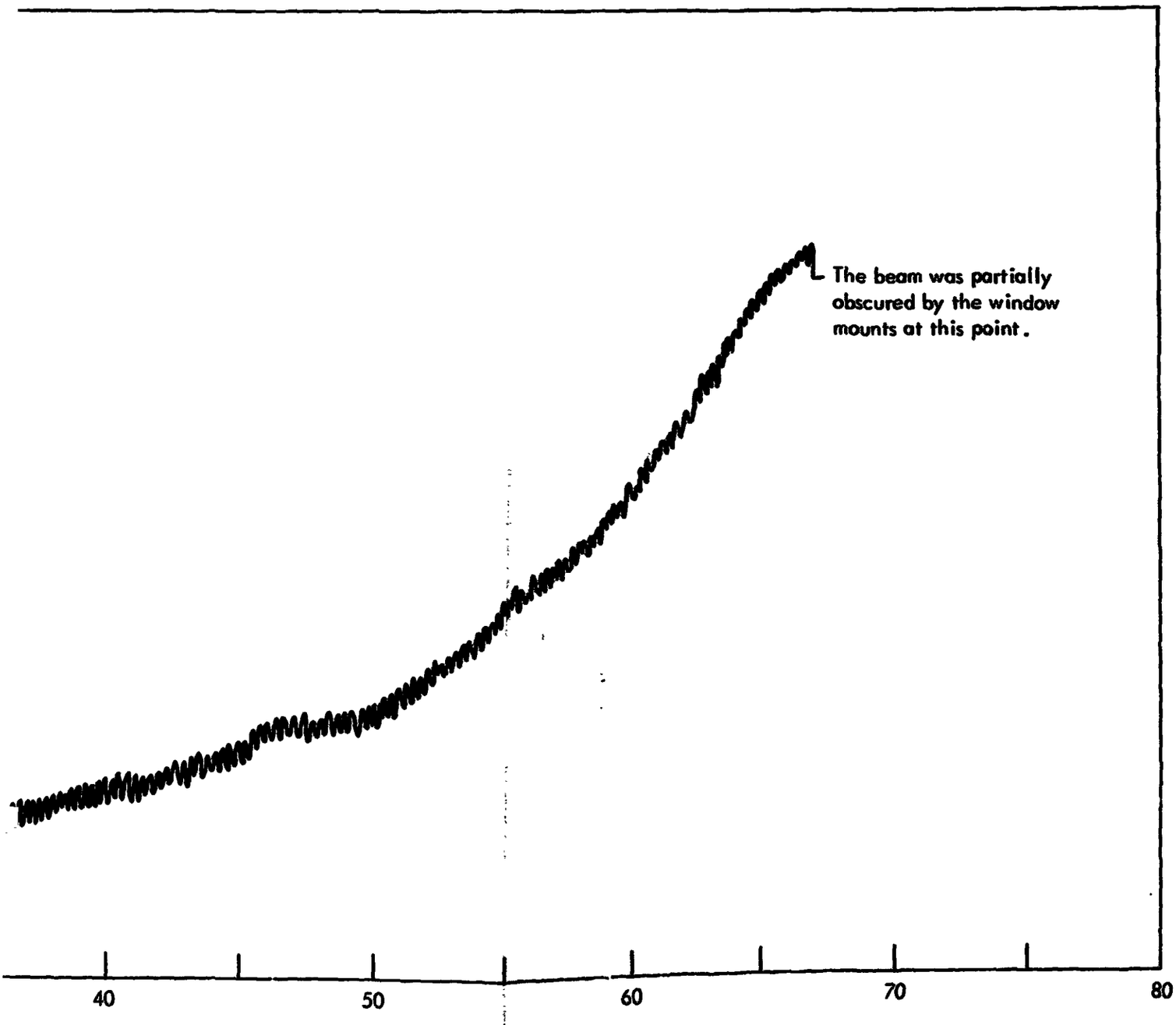

LE OF TILT - α (degrees)

xperimental fractional transmission through four optical flats of Germanium with the E-field parallel to the plane of incidence. The etalon effect is apparent throughout the range α.

FOLDOUT FRAME 2

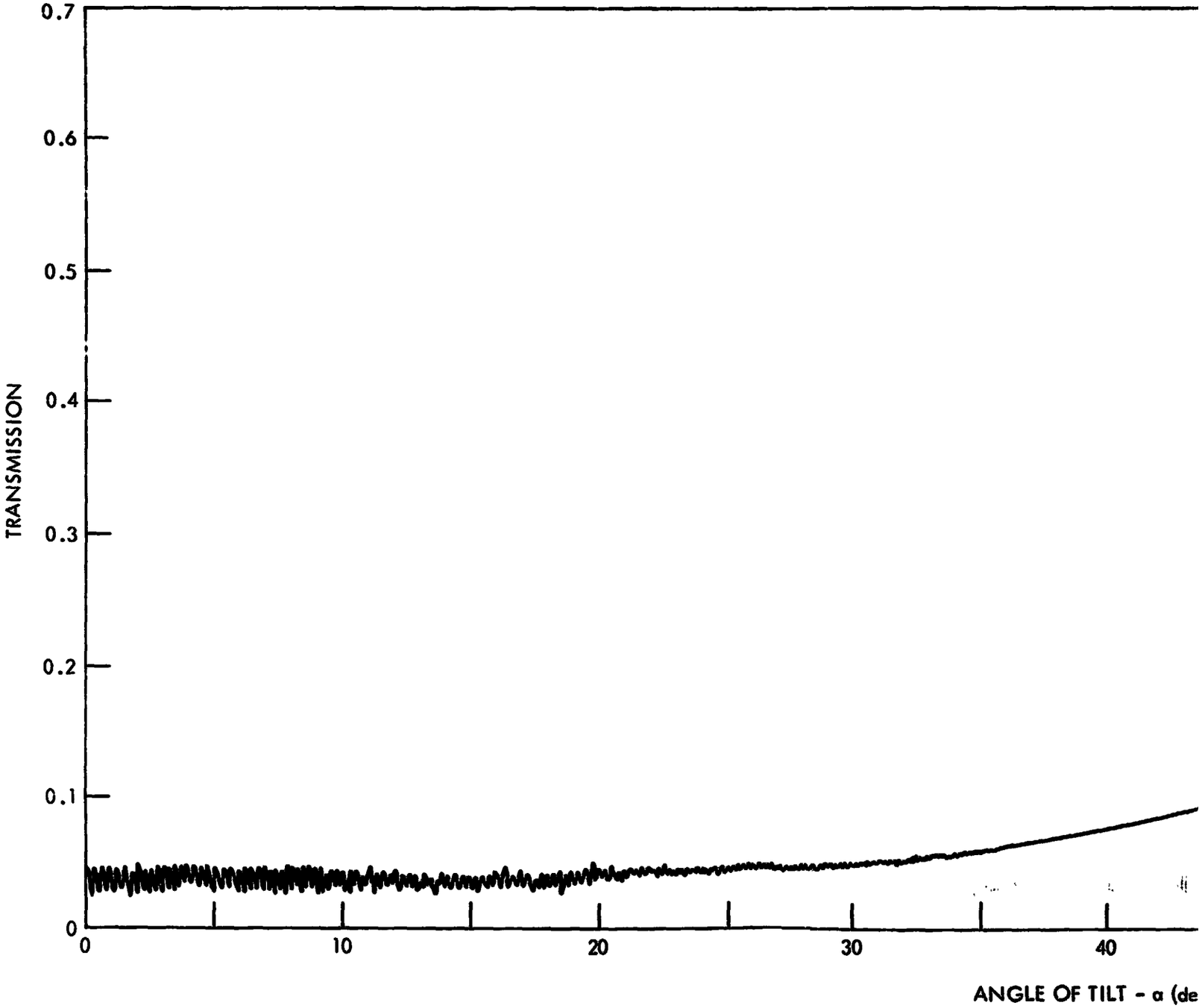

Figure 12. Experimental fraction

FOLDOUT FRAME /

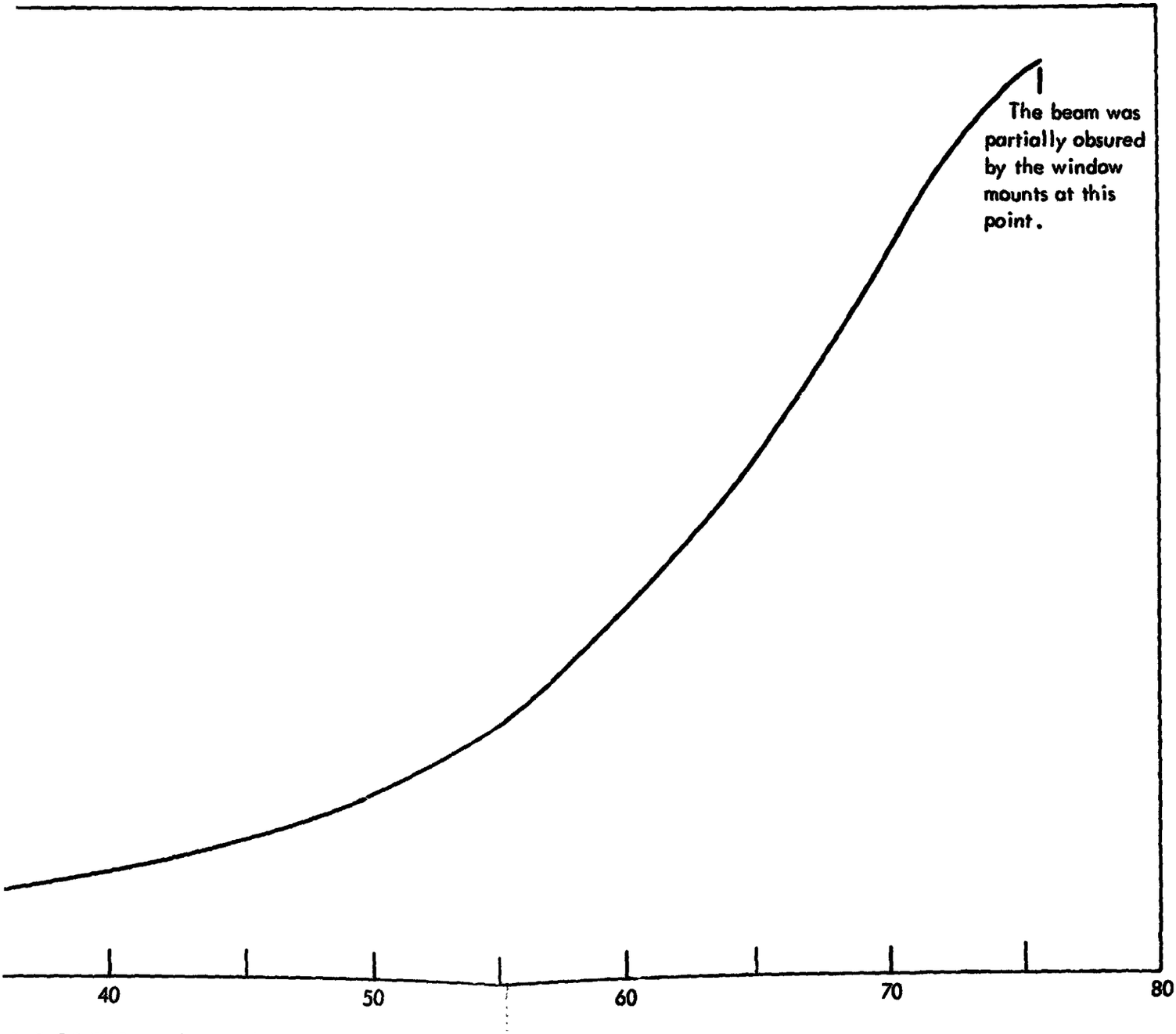

:perimental fractional transmission through the composite flat attenuator with the stationary masks and the E-field parallel to the plane of incidence.

FOLDOUT FRAME 2

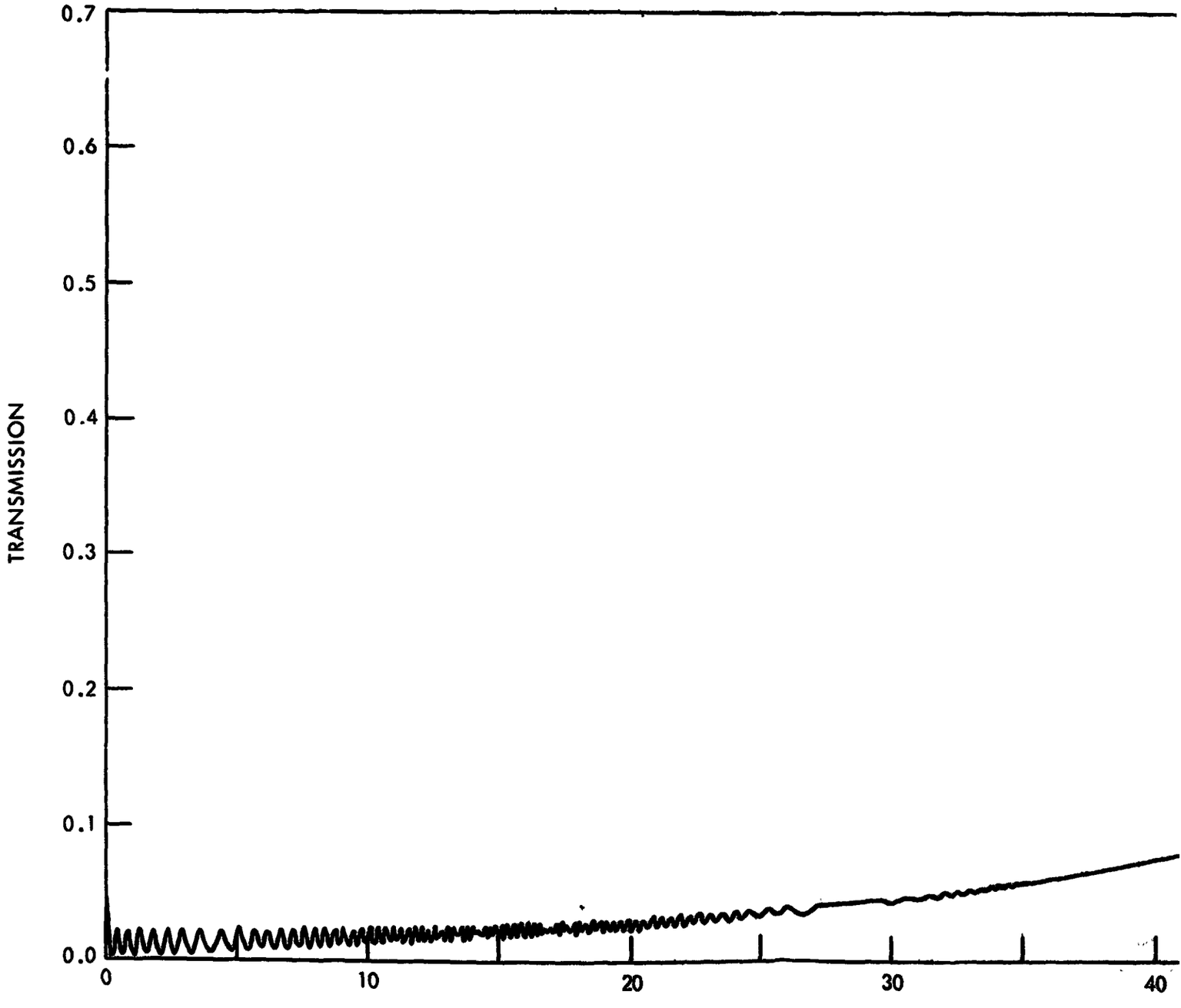

Figure 13. Theoretical tra

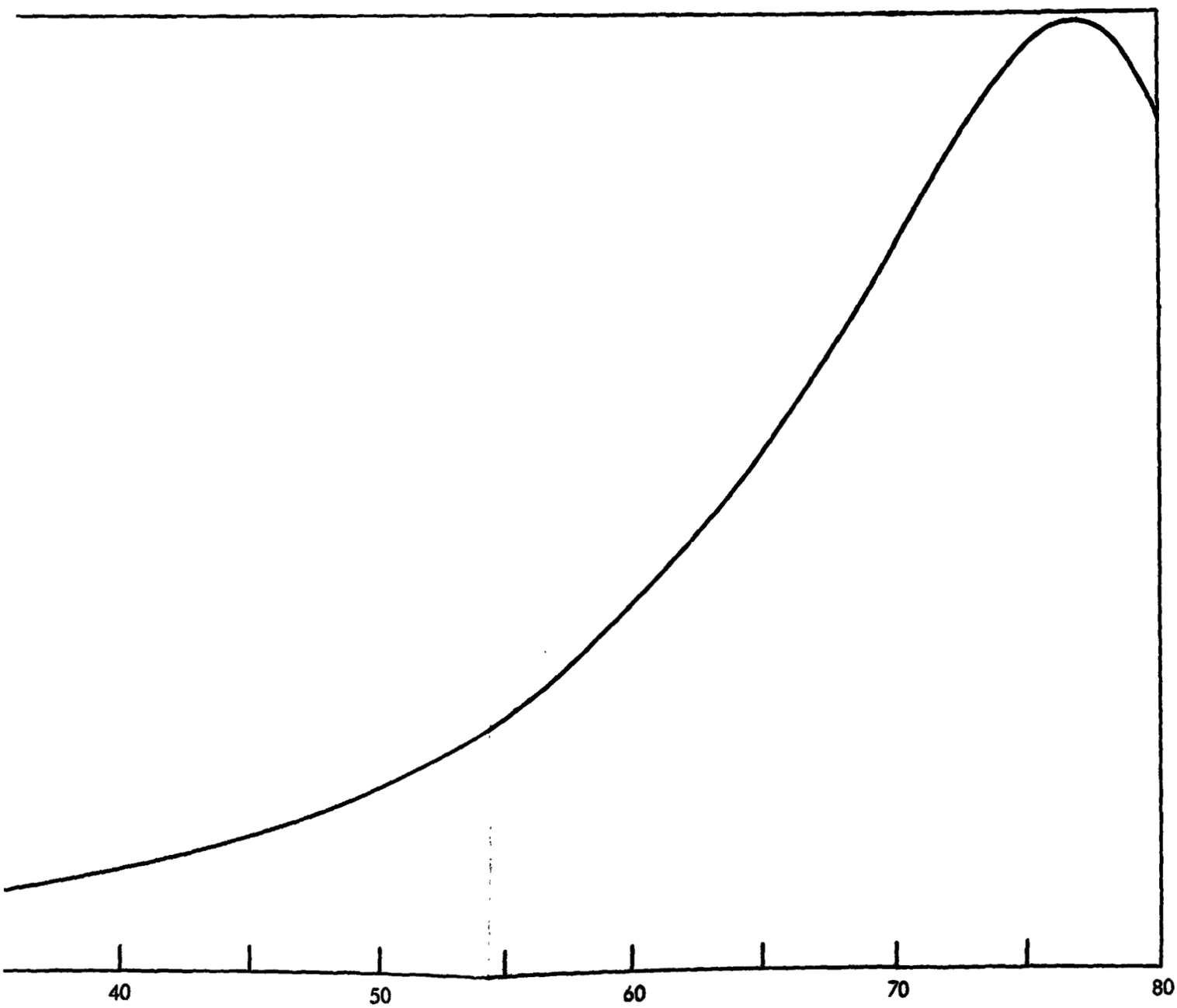

:GLE OF TILT - α (degrees)

heoretical transmission for the wedge attenuator predicting the interference effect of the strongest "secondary" beam at the output of the system.

FOLDOUT FRAME 2

V. CONCLUSION

It has been shown that the use of complementary wedges separated by an air gap improves the performance of an attenuator utilizing contra-rotating optical flats. Figures 8 and 10 show the double wedge attenuator with stationary masks to be satisfactory, in particular for the range of α from 25 to 75 degrees, and to compare favorably with the theoretical range of attenuation.

The physical constraints in adapting the wedge system to an existing device caused us to lose less than one dB of attenuation for large values of α, but not enough to destroy the usefulness of the system. In the region where the etalon effect is pronounced, one might suggest the use of antireflection coatings to suppress the multiple reflections. However, these optical coatings have an angular dependence and would have a detrimental effect on the transmission curves for regions outside the effective range.

Improvements in the present device would include enlarging the diameter and width of the aperture mounts to accommodate a larger wedge angle and/or air gap. Of course, the use of larger germanium flats would increase the cost of the device.

ACKNOWLEDGMENT

The authors are grateful to Clinton Winchester for his help in taking some of the data.

REFERENCES

1. W. Leeb, "Variable Beam Attenuator for the Infrared," Applied Optics, Vol. 13, January 1974, pp. 17-19.

2. R. L. Abrams and W. B. Gandrud, "A Variable 10.6-μ Attenuator", IEEE J. of Quantum Electronics, Vol. QE-5, April 1969, pp. 212-213.

3. J. H. McElroy, H. E. Walker, S. C. Flagiello, S. C. Cohen, and J. B. McDay, "Second Summary Design Report ATS-F Laser Communication Experiment Infrared Subsystems," NASA TM X-524-69-388, GSFC, July 1969.

4. T. M. Sporton, "Optical Transmission Through Windows Set Near the Brewster Angle," J. Sci. Instrum., Vol. 44, 1967, pp. 720-724.

5. F. A. Jenkins and H. E. White, Fundamentals of Optics, (McGraw-Hill Book Company, New York, 1957), pp. 510.

6. F. Horrigan, C. Klein, R. Rudko, and D. Wilson, "Windows for High-Power Lasers," Microwaves Magazine, Vol. 8, January 1969, pp. 68-76.

Appendix A

CALCULATION OF DISTANCE S

Fig. 2 has been enlarged in Fig. A1 to illustrate the method used to calculate the perpendicular distan ; S between the primary and "secondary" beams.

From the figure, S can be expressed as

$$S = a \cdot \text{Cos}\ \alpha \tag{1}$$

where α is the angle of incidence.

The parameter a can be found in terms of known parameters through a few simple identities. From Fig. A1

$$a = \frac{b}{\text{Cos}\ \beta}$$

$$b = 2c\ \text{Cos}(\beta - \theta)$$

$$c = f\ \text{Tan}\ \gamma$$

and

$$f = d\ \text{Cos}\ \theta$$

where d and θ are known parameters of the air gap width and wedge angle respectively. From the above equations we find

$$S = 2d\ \text{Cos}\ \theta\ \text{Tan}\ \gamma\ \text{Cos}(\beta - \theta)\frac{\text{Cos}\ \alpha}{\text{Cos}\ \beta} \tag{2}$$

where

$$\beta = \text{Arc sin}\left(\frac{\sin}{n_1}\right)$$

and

$$\gamma = \text{Arc sin}[n_1 \sin(\beta - \theta)].$$

Eq. (2) has been plotted in Fig. 4 and shows that the distance between the primary and "secondary" beams is substantially greater for the double wedge arrangement than for the optical flat.

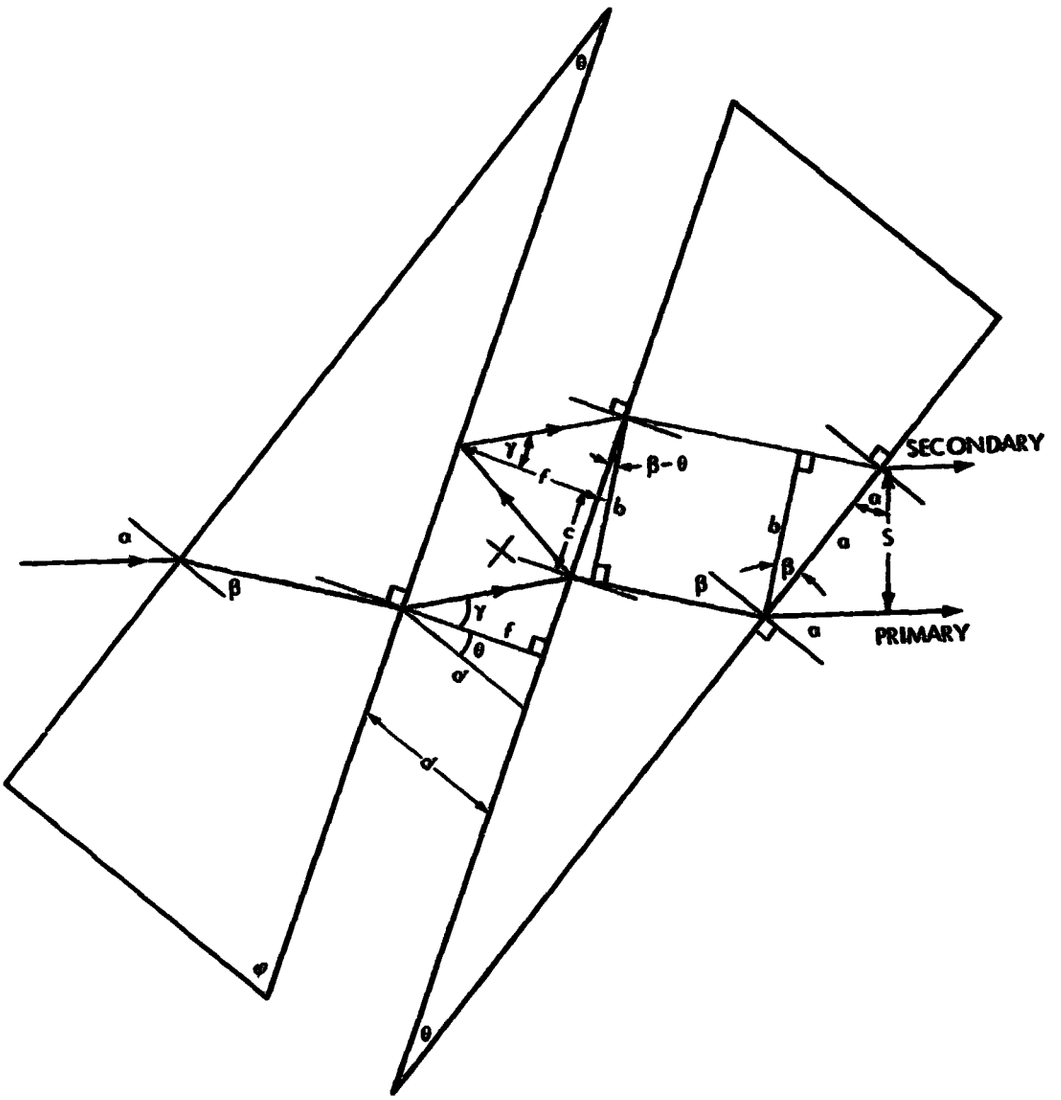

Figure A-1

Appendix B

POSITION OF THE PRIMARY BEAM RELATIVE TO THE OPTICAL AXIS OUTSIDE THE FIRST COMPOSITE FLAT

It may be interesting to note how the position of the primary beam changes outside the first pair of complementary wedges, relative to a stationary point or line such as the optical axis. This information may then aid in positioning the marks which will block extraneous secondary beams.

Fig. B1 has been drawn to illustrate the calculations involved. To find an expression for the variable distance R, which is labeled in the figure, we must first calculate ω, the distance along the wedge from the center line to where the primary beam leaves the wedge. Once ω is found it can be substituted into:

$$R = \left(\frac{t}{2}\text{Tan}\,\alpha - \omega\right)\text{Cos}\,\alpha \qquad (1B)$$

which can be obtained from Fig. B1.

The calculation of ω in terms of known parameters, involves a fair amount of trigonometry and we will have to refer to Fig. B1 quite often. Working initially with the second wedge of the composite flat it can be seen that

$$\omega = x' + y' \qquad (2B)$$

and

$$y' = k' \cot \theta.$$

If we equate similar triangles in the wedge we can obtain

$$\frac{k' + f'}{w} = \frac{\frac{z}{2} + \omega}{z}$$

therefore, $k' = w/z\ (z/2 + \omega) - f'$ and y' becomes

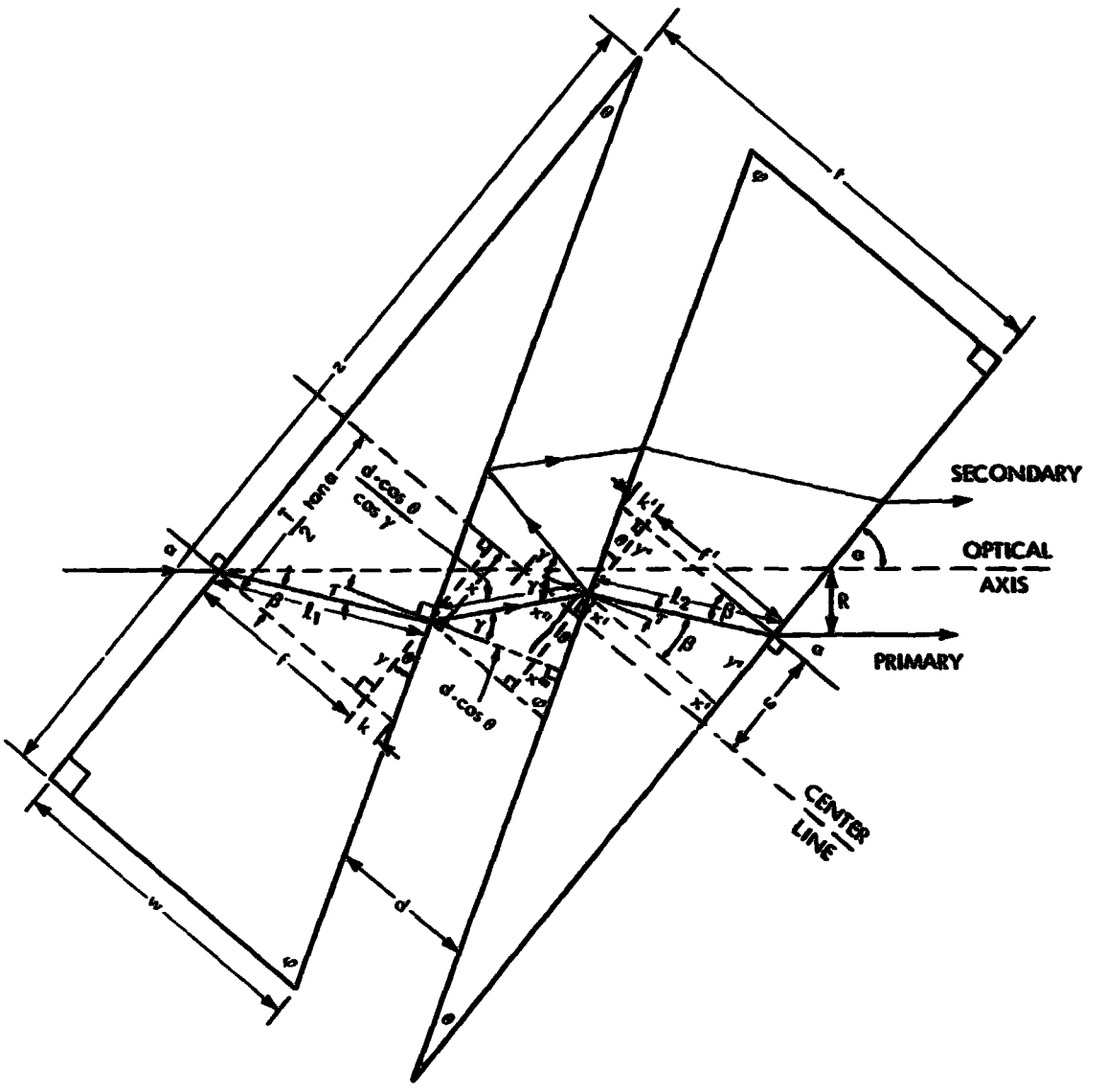

Figure B1

$$y' = \left[\frac{w}{z}\left(\frac{z}{2} + \omega\right) - f'\right] \text{Cot } \theta \qquad \text{(3B)}$$

There is still an unknown f' in the expression, therefore, let us redefine y', using the figure, as

$$y' = f' \text{ Tan } \beta$$

Multiplying Eq. (3B) by Tan β, Eq. (4B) by Cot θ and adding the two equations we find

$$y' = \frac{w}{z}\left[\frac{z}{2} + \omega\right] \frac{\text{Tan } \beta \text{ Cot } \theta}{\text{Tan } \beta + \text{Cot } \theta} \qquad \text{(5B)}$$

Now, if we can write x' as a function of known variables, we will be able to find an expression for ω from Eq. (2B).

From the figure we can see

$$x + x' = x'' + x''' \qquad \text{(6B)}$$

Using the law of Sines, an expression for x'' can be obtained.

$$\frac{x''}{\text{Sin } \gamma} = \frac{\dfrac{d \text{ Cos } \theta}{\text{Cos } \gamma}}{\text{Sin}(90^\circ + \theta)}$$

which yields $x'' = d \text{ Tan } \gamma$. By a similar calculation

$$x''' = \frac{d \text{ Cos}(\theta + \gamma) \text{ Sin } \theta}{\text{Cos } \gamma}.$$

From the figure

$$x = \frac{t}{2} \text{Tan } \alpha - y$$

and using the relation in Eq. (6B)

$$x = d \operatorname{Tan}\gamma + \frac{d \operatorname{Cos}(\theta + \gamma) \operatorname{Sin}\theta}{\operatorname{Cos}\gamma} - \frac{t}{2} \operatorname{Tan}\alpha + y \qquad (7B)$$

Now we need to calculate the parameter y in Eq. (7B). In the same fashion as y' was calculated, y can be found to be

$$y = \frac{w}{z}\left[\frac{z}{2} + \frac{t}{2}\operatorname{Tan}\alpha\right] \frac{\operatorname{Tan}\beta \operatorname{Cot}\theta}{\operatorname{Tan}\beta + \operatorname{Cot}\theta} \qquad (8B)$$

Substituting Eqs. (5B), (7B) and (8B) into Eq. (2B), we can, after some simplification, find

$$\alpha = \frac{w\psi + d \operatorname{Tan}\gamma + \frac{t}{2}\operatorname{Tan}\alpha\left(\frac{w}{z}\psi - 1\right) + d \operatorname{Cos}(\theta + \gamma)\frac{\operatorname{Sin}\theta}{\operatorname{Cos}\gamma}}{1 - \psi\frac{w}{z}} \qquad (10B)$$

where

$$\psi = \frac{\operatorname{Cot}\theta \operatorname{Tan}\beta}{\operatorname{Cot}\theta + \operatorname{Tan}\beta}$$

$$\gamma = \operatorname{Sin}^{-1}[n_1 \operatorname{Sin}(\beta - \theta)]$$

and t, w and d are as defined in Fig. B1.

If Eq. (1B) is plotted versus angle of incidence, α, the distance R would be shown to increase monotonically, i.e., the primary beam continuously moves away from the optical axis for increasing values of α.

Appendix C

CALCULATION OF OPTICAL PATH LENGTHS ℓ_1 AND ℓ_2

The calculation of ℓ_1 and ℓ_2 is simplified by utilizing the result of Appendix B. The paths of the primary beam through the two wedges have been labeled in Fig. B1. From the diagram, the two lengths may be represented as

$$\ell_1 = \frac{y}{\sin \beta} \tag{1C}$$

and

$$\ell_2 = \frac{y'}{\sin \beta}. \tag{2C}$$

Using Appendix B, we can obtain y and y' from Eqs. (8B) and (5B), respectively to obtain

$$\ell_1 = \frac{w}{z}\left[\frac{z}{2} + \frac{T}{2}\tan \alpha\right] \frac{\psi}{\sin \beta}$$

$$\ell_2 = \frac{w}{z}\left[\frac{z}{2} + \omega\right] \frac{\psi}{\sin \beta}$$

where ω is given by Eq. (10B) and

$$\psi = \frac{\tan \beta \cot \beta}{\tan \beta + \cot \beta}.$$